Check for updates

Chemistry – A European Journal

ChemEurJ Chemistry Europe European Chemical Societies Publishing

RESEARCH ARTICLE

Light-Powered Atroposelective Ratcheting via Excited-State Donor–Acceptor Interactions

Chun-Wei Chiu[1] | Hsiu-Feng Lu[2] | Sudhakar Narra[3] | Eric Wei-Guang Diau[3] | Chun-Fu Chang[3] | Chao-Ping Hsu[2,4] | Jye-Shane Yang[1,5]

[1]Department of Chemistry, National Taiwan University, Taipei, Taiwan | [2]Institute of Chemistry, Academia Sinica, Taipei, Taiwan | [3]Department of Applied Chemistry and Institute of Molecular Science, National Yang Ming Chiao Tung University, Hsinchu, Taiwan | [4]Division of Physics, National Center for Theoretical Sciences, Taipei, Taiwan | [5]Center For Emerging Material and Advanced Devices, National Taiwan University, Taipei, Taiwan

Correspondence: Chun-Fu Chang (chunfuc@nycu.edu.tw) | Chao-Ping Hsu (cherri@sinica.edu.tw) | Jye-Shane Yang (jsyang@ntu.edu.tw)

Received: 8 April 2026 | **Revised:** 19 June 2026 | **Accepted:** 23 June 2026

Keywords: atropisomerism | donor–acceptor systems | light-powered ratchets | pentiptycene

ABSTRACT

A light-powered atroposelective ratcheting system based on a desymmetrized pentiptycene scaffold is reported. This structural framework enforces templated donor–acceptor (D–A) arrangements capable of distinguishing between rapidly equilibrating atropisomers, enabling atroposelective $Z \rightarrow E$ photoisomerization that selectively suppresses the consumption of one atropisomer and leads to its accumulation under continuous irradiation. Ultrafast transient spectroscopic studies and theoretical calculations reveal that this photochemical atroposelectivity arises from electronic interactions between the donor and acceptor moieties in the excited state. Such an atroposelective ratchet could potentially be harnessed to construct light-driven rotary molecular motors (LRMMs). These results highlight the role of conformer-dependent photochemistry in achieving precise photochemical control over molecular motion.

1 | Introduction

Light-powered ratcheting converts photonic energy into chemical energy, enabling chemical systems to operate away from thermodynamic equilibrium [1, 2]. Such behavior is typically achieved by coupling an equilibrating system to specific photochemical transformations through the incorporation of photo-responsive units. Light-powered ratcheting has been exploited in stimuli-adaptive dynamic covalent libraries [3–10], dissipative supramolecular assemblies [11–21], and light-driven rotary molecular motors (LRMMs) based on overcrowded double bonds [22–24].

Despite these advances, the operation of ratcheting systems generally requires that thermal equilibration of the ratcheted process be sufficiently slow so that its equilibrium can be lifted under kinetically controlled conditions. This requirement poses a major challenge for rapidly equilibrating systems, such as atropisomerism around fast-rotating single bonds. According to LaPlante and coworkers [25], bonds with rotational barriers below 20 kcal/mol are classified as fast-rotating and undergo rapid atropisomeric equilibration. Atroposelective ratcheting of such bonds underpins the operation of autonomous rotary molecular motors and has been realized in several chemically powered systems [26–30]. These systems typically rely on stereoselective catalytic steps to introduce a kinetic bias, thereby driving the system away from equilibrium under Curtin–Hammett control [31]. In contrast, light-powered atroposelective ratcheting remains far less explored, largely because of the limited number of strategies available for deliberately introducing atroposelectivity into photochemical reactions. Recently, Curcio and coworkers reported the first example of an autonomous LRMM that undergoes directional rotation about a single bond [32]. Operation of this system relies on light-powered ratcheting of the atropisomeric composition away from equilibrium, which

© 2026 Wiley-VCH GmbH

in turn governs the directionality of rotation. While this work represents an important advance in the field, the system does not incorporate dedicated structural features to strongly enforce atroposelectivity, which may contribute to the relatively modest ratcheting efficiency observed.

To address the challenge of achieving strategic control over photochemical atroposelectivity, we propose a structural framework capable of translating conformer-dependent photochemistry into atroposelective ratcheting. Previously, we reported a light-gated molecular brake (**1br**), in which the rate of internal C—C bond rotation can be modulated by *E,Z*-photoisomerization [33]. As depicted in Figure 1a, **1br** is a stilbene derivative incorporating an H-shaped, C_2-symmetric pentiptycene scaffold with two U-shaped cavities [34]. Rotation about the pentiptycene–styryl bond is unhindered in the *E* form but sterically hindered in the *Z* form, in which the styryl group is partially inserted into one of the U-shaped cavities. The rate of this C—C bond rotation can be modulated photochemically by *E,Z*-photoisomerization, which switches the system between fast- and slow-rotating states. Because the C—C bond rotation in this system is coupled to a photochromic reaction, it provides a promising platform for engineering a light-powered atroposelective ratchet. Specifically, desymmetrization of the pentiptycene scaffold by substitution, as in **1ra** (Figure 1b), generates two distinct atropisomers (*syn* and *anti*) in the *Z*-**1ra** isomer because the two cavities are inequivalent. The key requirements for constructing a light-powered atroposelective ratchet can thus be satisfied, provided that the *syn-Z* and *anti-Z* atropisomers can be distinguished photochemically. This distinction can be achieved by exploiting templated excited-state donor–acceptor (D–A) interactions [35–38] in *syn-Z*-**1ra**, where the D–A motifs are in close proximity. Excited-state D–A interactions are known to drive light-trapping of metastable D–A ground-state assemblies, demonstrating that transient excited-state interactions can kinetically perturb ground-state equilibria [19]. Consistent with this concept, we find that excited-state D–A interactions in the *syn-Z*-**1ra** atropisomer effectively suppress its $Z \rightarrow E$ photoisomerization, leading to accumulation of this atropisomer under continuous irradiation, as schematically illustrated in Figure 1b. In contrast to Curcio's system, which is primarily sterically directed, this system represents, to the best of our knowledge, the first example of a light-powered atroposelective ratchet in which atroposelectivity is electronically gated through conformer-dependent photochemistry.

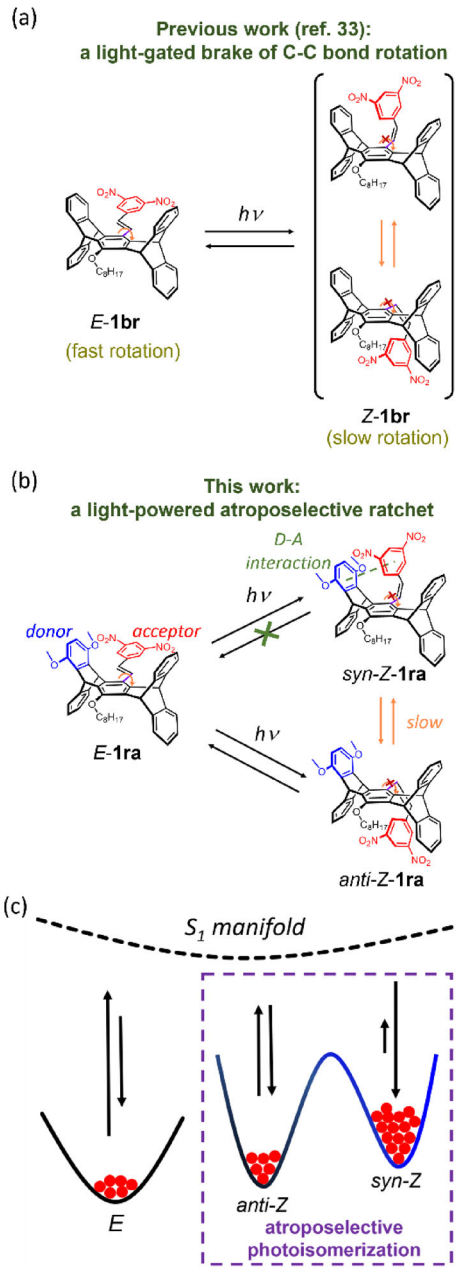

FIGURE 1 | Structural design of (a) the previously reported light-gated molecular brake **1br**, featuring a switchable rotation rate about a C—C bond, [33] and (b) the light-powered atroposelective molecular ratchet **1ra** developed in this work. (c) Working principle of the light-powered atroposelective molecular ratchet **1ra**. Note that the energetic ordering of the *syn* and *anti* atropisomers of *Z*-**1ra** is temperature dependent.

2 | Results and Discussion

2.1 | Synthesis and Structural Analysis

The synthesis of compound **1ra** was accomplished via a Heck coupling reaction to construct its stilbene backbone, affording exclusively the *E* isomer. Details of the synthetic procedures are described in Supporting Information (Scheme S1). Photoisomerization under 365 nm irradiation in toluene converted 79% of **1ra** to the *Z* isomer, and the configurational isomers could be separated with preparative HPLC. Alternatively, one-way $E \rightarrow Z$ isomerization could be done via photosensitization with fluorenone, enabling quantitative conversion to *Z*-**1ra** [39]. Notably, **1ra** is chiral due to desymmetrization of the pentiptycene scaffold. Since the inherent chirality of *Z*-**1ra** does not affect its atropochemical behaviors, all studies in this work were conducted using the racemate as a proof of concept.

Structural analysis of **1ra** was performed with x-ray crystallography, DFT calculations (B3LYP/6-31G(d)), and by NMR spectroscopy. The NMR signal assignments were further assisted by 2D NMR methods (Figures S1–S3). Considering the rotamerism of both the pentiptycene-styryl C—C bond and the pentiptycene-alkoxyl C—O bond, there are four near isoenergetic

15213765, 0, Downloaded from https://chemistry-europe.onlinelibrary.wiley.com/doi/10.1002/chem.71388 by National Yang Ming Chiao Tung, Wiley Online Library on [30/07/2026]. See the Terms and Conditions (https://onlinelibrary.wiley.com/terms-and-conditions) on Wiley Online Library for rules of use; OA articles are governed by the applicable Creative Commons License

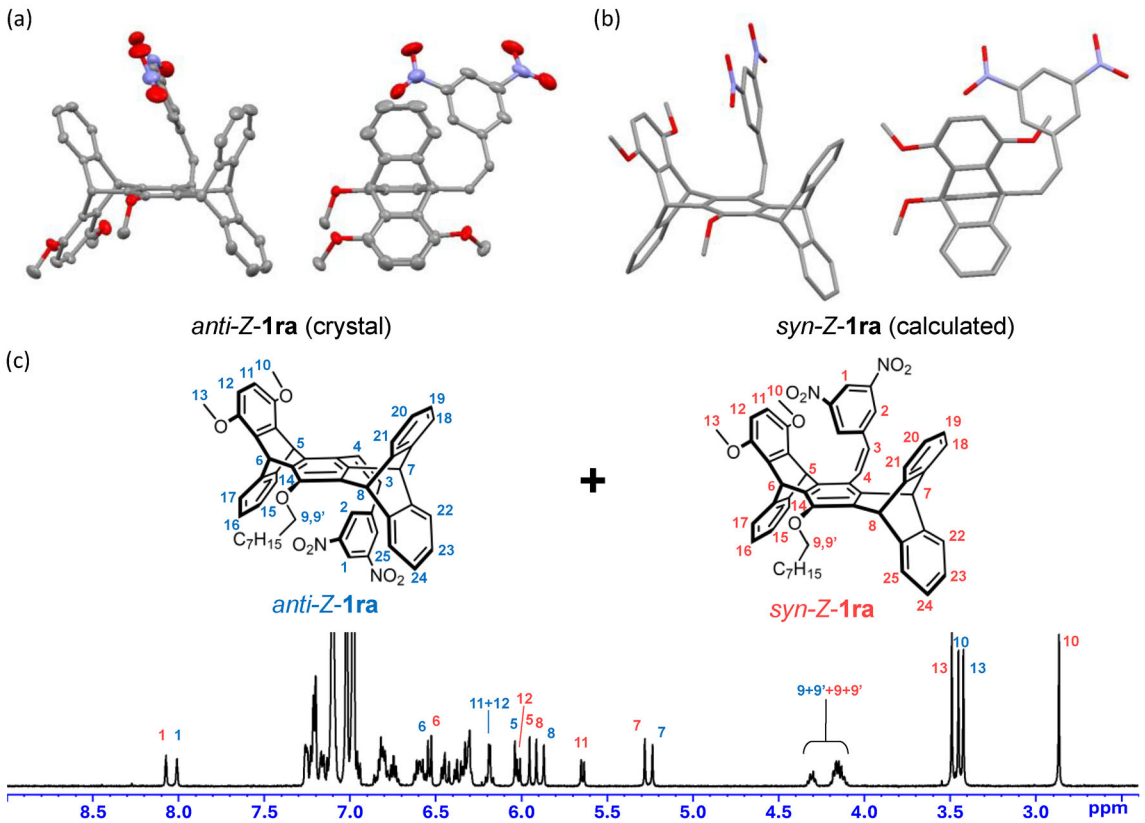

FIGURE 2 | Molecular structures and ^{1}H NMR spectrum of *Z*-**1ra**: (a) the *anti* form observed in x-ray crystal structure and (b) the *syn* form of DFT-optimized structures, where the octyloxy group is replaced with methoxy for simplicity, and (c) the ^{1}H NMR spectrum (500 MHz, toluene-d_8) determined at ambient temperature showing the presence of both *syn* and *anti* forms.

conformers for *Z*-**1ra** (Figure S4). However, only the *anti-Z*-**1ra** form is observed in single crystals grown from *Z*-**1ra** solutions (Figure 2a), presumably because the relatively large dipole moment of this atropisomer (9.21 D, predicted by DFT, Table S1) promotes its selective crystallization from the solution-state atropisomeric mixture [40]. For comparison, the DFT-derived *syn-Z*-**1ra** is shown in Figure 2b. In both *syn* and *anti* forms, steric hindrance between the dinitrophenylene and pentiptycene moieties constrains the rotation about the pentiptycene-styryl C—C bond. Consequently, signals corresponding to the *syn* and *anti* forms are resolvable on the ^{1}H-NMR spectrum of *Z*-**1ra** at 298 K, as shown in Figure 2c. The significantly upfield-shifted methoxy signal at 2.86 ppm was assigned to the methoxy proton H_{10} of *syn-Z*-**1ra**, which suffers from anisotropic magnetic shielding induced by the dinitrophenylene moiety. Although no NOE correlation was observed between the methoxy signals and the dinitrophenylene protons, ratios of signal integration allowed the resonances at 8.01 and 8.07 ppm to be assigned to H_1 of *anti-* and *syn-Z*-**1ra**, respectively.

2.2 | Characterization of C—C Bond Atropisomerism

The kinetic and thermodynamic properties of the conformer stereodynamics of *Z*-**1ra** are of fundamental importance in the context of ratcheting. Therefore, these issues were investigated in detail with multiple NMR methods. Rotations about the pentiptycene-alkyloxy C—O bond are rapid, since they are not sterically hindered. Consequently, the C—O rotamerism is always considered to be at equilibrium, and the following discussion focuses exclusively on rotamerism about the pentiptycene-styryl C—C bond.

The exchange between *anti-* and *syn-Z*-**1ra** through C—C bond rotation is evident from the emergence of off-diagonal signals on the 2D-EXSY spectrum of *Z*-**1ra** at 298 K (Figure 3a). DFT calculations predicted a *syn–anti* barrier of 16.4 kcal/mol as an average outcome of multiple possible pathways (Figure S5 and Table S2). The kinetics of this exchange were further evaluated experimentally with variable-temperature NMR (VT-NMR) spectroscopy. As shown in Figure 3b, gradual broadening of the H_{10} signal of the *syn* form at elevated temperatures indicated enhanced *syn–anti* exchange due to accelerated C—C bond rotation. Exchange rates at each temperature were extracted from spectral line-shape fitting and subjected to Eyring analysis, yielding a free energy barrier of 15.6 ± 0.9 kcal/mol for *syn–anti* interconversion at 298 K (Table 1 and Figure S6b), in reasonable agreement with the DFT-calculated value.

The atropisomeric equilibrium constant ($K_{sa} = [syn]_{eq}/[anti]_{eq}$) was readily determined through integration of the corresponding NMR signals. The K_{sa} value was determined as 1.12 in toluene-d_8 at 298 K, reflecting a slight preference for the *syn* form, which is in excellent agreement with DFT calculations

15213765, 0, Downloaded from https://chemistry-europe.onlinelibrary.wiley.com/doi/10.1002/chem.71388 by National Yang Ming Chiao Tung, Wiley Online Library on [30/07/2026]. See the Terms and Conditions (https://onlinelibrary.wiley.com/terms-and-conditions) on Wiley Online Library for rules of use; OA articles are governed by the applicable Creative Commons License

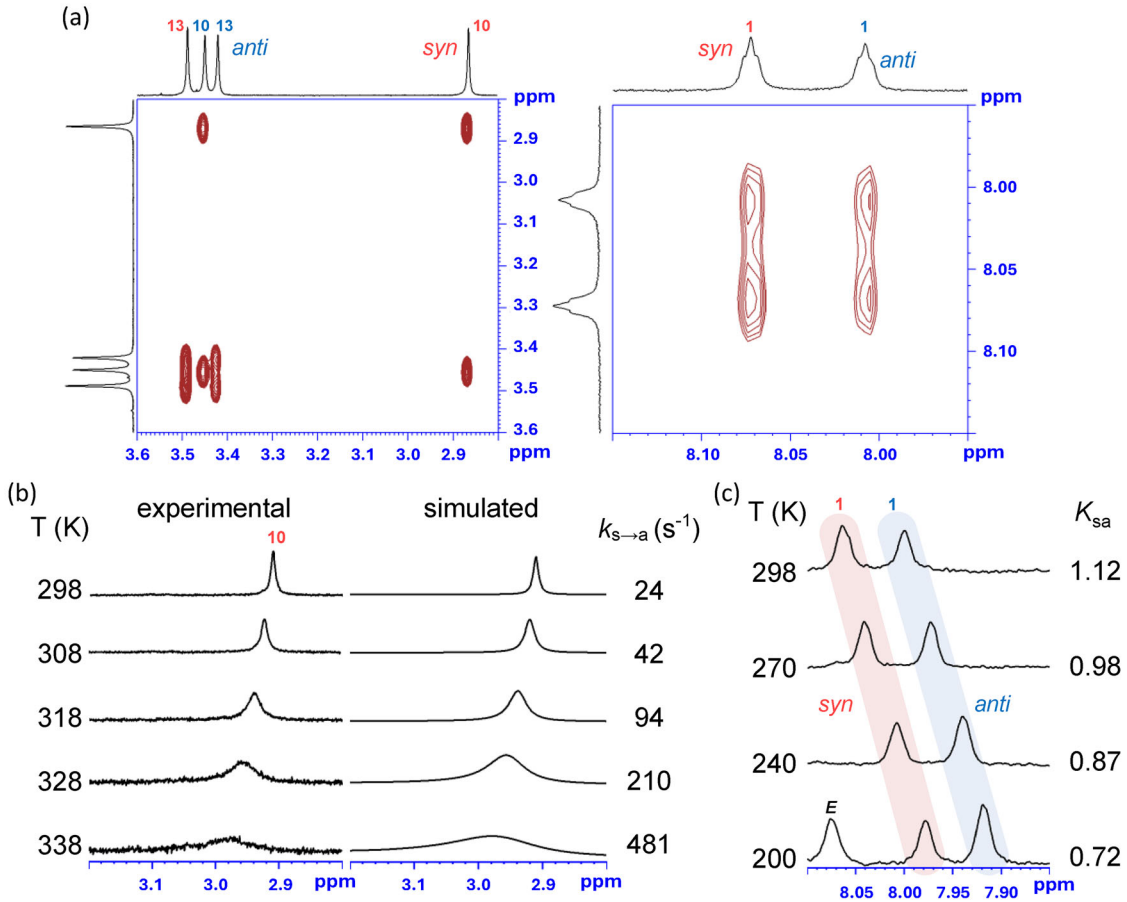

FIGURE 3 | (a) Selected slices of the 2D EXSY spectrum of *Z*-**1ra** (500 MHz, toluene-d_8). (b) Experimental and simulated VT ^{1}H-NMR spectra of *Z*-**1ra** at the high-temperature range (400 MHz, toluene- d_8). (c) VT ^{1}H-NMR spectra of *Z*-**1ra** (containing residual *E* isomers) at the low-temperature range (400 MHz, toluene-d_8).

TABLE 1 | Kinetic and thermodynamic parameters of the *syn*–*anti* atropisomeric exchange of *Z*-**1ra** in toluene-d_8 at 298 K.

Kinetic		**Thermodynamic**	
$\Delta H^{\ddagger}_{s\to a}$ (kcal/mol)	14.5 ± 0.9[a]	ΔH^{o}_{sa} (kcal/mol)	0.53 ± 0.04
$\Delta S^{\ddagger}_{s\to a}$ (cal/mol K)	−3.7 ± 0.2	ΔS^{o}_{sa} (cal/mol K)	1.98 ± 0.04
$\Delta G^{\ddagger}_{s\to a}$ (kcal/mol)	15.6 ± 0.9	ΔG^{o}_{sa} (kcal/mol)	−0.06 ± 0.05
$k_{s\to a}$[b] (s^{-1})	21	K_{sa} = $[syn]_{eq}/[anti]_{eq}$	1.12 (0.72)[c]

[a]Errors correspond to fitting uncertainties.
[b]Estimated with Eyring equation.
[c]at 200 K.

that predicted a K_{sa} of 1.16 (Table S1). Interestingly, the equilibrium shifted toward the *anti* form at lower temperatures, with K_{sa} decreasing to 0.72 at 200 K in the same solvent (Figure 3c). This trend is presumably attributed to enhanced solvation toward the more polar *anti* form at low temperatures, consistent with the equilibrium condition in CD_2Cl_2 at 298 K, which also slightly favors the *anti* form (K_{sa} = 0.88, Figure S7).

The thermodynamic parameters ΔH^{o}_{sa}, ΔS^{o}_{sa}, and ΔG^{o}_{sa} associated with *anti-syn* exchange were obtained with Van't Hoff analysis of the temperature-dependent K_{sa} values (Figure S8). The results, summarized in Table 1, indicated that the *anti* form is slightly favored enthalpically, whereas the entropic contributions favor the *syn* form, which accounts for the observed temperature dependence of K_{sa}. These energetic features imply the absence of stabilizing D–A interactions in *syn-Z*-**1ra** in the ground state. This argument is also supported by the absorption spectrum of *Z*-**1ra**, which does not exhibit charge-transfer (CT) absorption bands (Figure S9a). This behavior could be attributed to the structural offset between the D–A units in *syn-Z*-**1ra**, evident in Figure 2b.

15213765, 0, Downloaded from https://chemistry-europe.onlinelibrary.wiley.com/doi/10.1002/chem.71388 by National Yang Ming Chiao Tung, Wiley Online Library on [30/07/2026]. See the Terms and Conditions (https://onlinelibrary.wiley.com/terms-and-conditions) on Wiley Online Library for rules of use; OA articles are governed by the applicable Creative Commons License

TABLE 2 | Photochemical properties of **1ra**.

T (K)	298	200
$\Phi_{E\to Z}$[a]	0.06	—
$\Phi_{Z\to E}$[a]	0.01	—
$(Z)/(E)$[b]	79:21	73:27
R_{sa}[b]	1.12	1.33
$K_r = R_{sa}/K_{sa}$[b]	1.00	1.85

[a]In *n*-hexane.
[b]Under 365-nm PSS in toluene-d_8.

2.3 | Light-Powered Ratcheting

The trial for light-powered ratcheting of C—C atropisomerism was performed by irradiating **1ra** in toluene-d_8 with 365 nm LED flashlight, while monitoring the evolution in atropisomeric composition by ^{1}H NMR spectroscopy. Based on the free energy barrier of 15.6 kcal/mol associated with *syn*-to-*anti* interconversion (Table 1), the half-life ($t_{1/2}$) for thermal equilibration at 298 K was estimated as 0.02 s (Table S3). This suggests that the off-equilibrium compositions generated by light irradiation are too short-lived to be characterized at 298 K. Indeed, the observed atropisomeric ratio (R_{sa} = [*syn*]/[*anti*]) was identical to K_{sa} after 1 h irradiation at 298 K. To suppress thermal re-equilibration, the experiment was repeated at 200 K, where the estimated half-life of 1.1 h (Table S3) is sufficiently long for characterization by NMR spectroscopy. Figure 4a shows the schematic representation of the actual experimental setup (Figure S10) for the low-temperature trials. The sample (1 mM) was slowly cooled to 200 K in an acetone cooling bath. After 1 h of irradiation at 200 K, the isomeric composition of the system reached a photo-stationary state (PSS), after which no further changes were observed upon prolonged irradiation. The sample was then immediately transferred, maintained at 200 K in a Dewar flask, to an NMR spectrometer pre-cooled to 200 K, where spectra were recorded.

Figure 4b shows the ^{1}H NMR spectra of *E*- and *Z*-**1ra**, along with the 365 nm PSS at 200 K. At the PSS, a *Z*:*E* ratio of 73:27 with R_{sa} = 1.33 was observed. Compared to the equilibrium condition at 200 K (K_{sa} = 0.72), the corresponding ratcheting constant (K_r) can be calculated as R_{sa}/K_{sa} = 1.85, reflecting significant enrichment of the *syn* compared to the equilibrium state. This demonstrated that the C—C atropisomeric equilibrium of *Z*-**1ra** could indeed be perturbed by light irradiation, confirming the light-powered ratcheting behavior of **1ra**. Note that no photodegradation of **1ra** was observed in this experiment (Figure S12). The photochemical properties of **1ra**, including the ratcheting behaviors, are summarized in Table 2, with the corresponding quantum yields of isomerization ($\Phi_{E\to Z}$ and $\Phi_{Z\to E}$) at 298 K also provided for reference.

Furthermore, thermal equilibration of the off-equilibrium state was also characterized. As shown in Figure 4c, a sample irradiated for 30 min and then left at 200 K in the dark for 2 h exhibited a gradual decrease in R_{sa}, from 1.15 to 0.97. By monitoring the relaxation of R_{sa} toward K_{sa}, $t_{1/2}$ of equilibration was determined to be 2.4 h (Figure S13 and Table S4). This value is longer than that

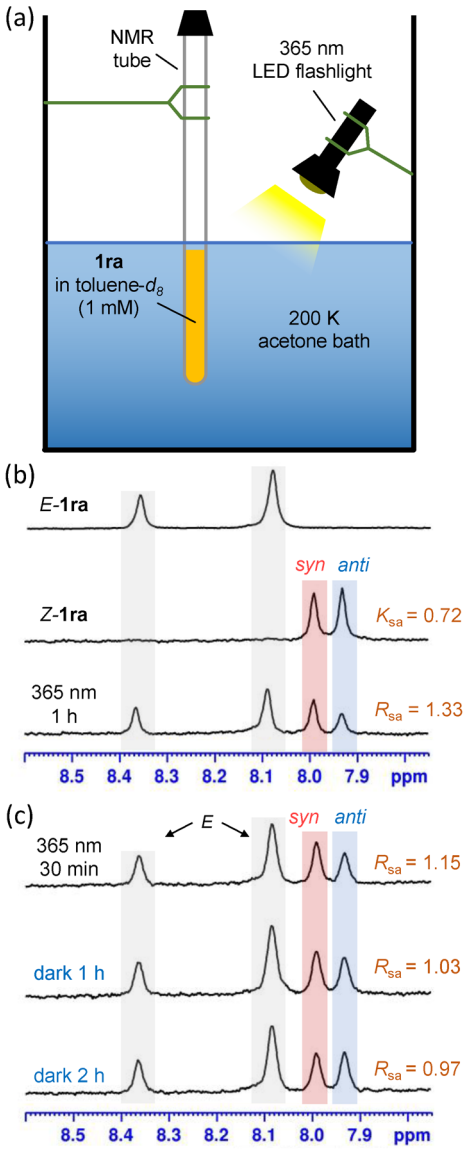

FIGURE 4 | Evaluation of *syn*:*anti* ratio (R_{sa}) of *Z*-**1ra** in toluene-d_8 at 200 K: (a) experimental setup for the light-powered ratcheting experiments conducted at 200 K; (b) ^{1}H NMR spectra (400 MHz) of *E*-**1ra**, *Z*-**1ra**, and their PSS at 365 nm; (c) evolution of R_{sa} in the dark, showing thermal re-equilibration from the off-equilibrium state.

estimated by VT-NMR spectroscopy, although it remains in the same order of magnitude. This deviation presumably arises from the fact that the VT-NMR experiments were conducted at elevated temperatures (298–338 K), and linear extrapolation of this trend to 200 K may not be valid. Nevertheless, such a long lifetime precluded the possibility for the observed signal enhancement to arise from light-induced nuclear polarization (photo-CIDNP), which typically relaxes within seconds [41].

2.4 | Mechanistic Studies

There are two possible origins for the light-powered ratcheting behavior in the enrichment of *syn*-*Z*-**1ra** during *E*,*Z*-photoisomerization: either *E*-**1ra** preferentially forms *syn*-*Z*-**1ra** during $E \to Z$ isomerization, or *anti*-*Z*-**1ra** undergoes $Z \to$

15213765, 0, Downloaded from https://chemistry-europe.onlinelibrary.wiley.com/doi/10.1002/chem.71388 by National Yang Ming Chiao Tung, Wiley Online Library on [30/07/2026]. See the Terms and Conditions (https://onlinelibrary.wiley.com/terms-and-conditions) on Wiley Online Library for rules of use; OA articles are governed by the applicable Creative Commons License

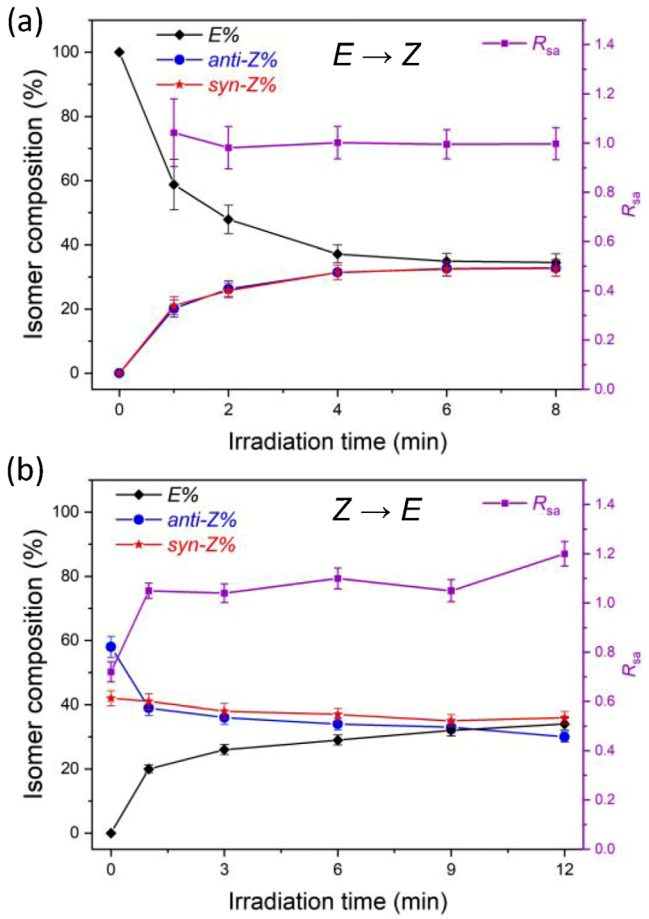

FIGURE 5 | Evolution in relative compositions of the three stereoisomers during direct irradiation (λ_{irr} = 365 nm) of (a) *E*-**1ra** and (b) *Z*-**1ra** at 200 K in toluene-d_8. Standard errors are estimated according to the signal-to-noise ratio in the spectra (see Figures S14 and S15 for original spectra).

E isomerization more rapidly than *syn-Z*-**1ra**, leading to its preferential depletion. To clarify the origin, we have examined the photochemical reactivities of the three stereoisomers of **1ra** (i.e., *E*-**1ra**, *syn-Z*-**1ra**, and *anti-Z*-**1ra**) to probe the stereoselectivities in both the photochemical $E \rightarrow Z$ and $Z \rightarrow E$ processes.

The $E \rightarrow Z$ process was first examined by monitoring the compositional evolution of the three stereoisomers during short irradiation periods at 200 K. As shown in Figure 5a, the *anti-Z* and *syn-Z* isomers formed in nearly equal amounts within the first 8 min of irradiation, and the R_{sa} values fluctuated around unity. This implies that the $E \rightarrow Z$ photoisomerization of **1ra** exhibits little intrinsic stereoselectivity. Although the $E \rightarrow Z$ process increases the R_{sa} value from the equilibrium value of 0.72 to approximately 1.00, this alone does not account for the reversal in atropisomeric preference ($R_{sa} > 1.00$) observed under prolonged irradiation. Evidently, the stereoselectivity that leads to the accumulation of the *syn-Z* isomer **1ra** under continuous irradiation arises from a different photochemical step.

For the stereoselectivities in the $Z \rightarrow E$ process, the compositional evolution during direct photoisomerization of *Z*-**1ra** was monitored to evaluate the relative photochemical reactivities between *syn-* and *anti-Z*-**1ra** (Figure 5b). In the early stages of the reaction (first 9 min), the abundance of *anti-Z*-**1ra** decreased significantly by 24%, whereas *syn-Z*-**1ra** only showed a minor decline of 8%. Apparently, *anti-Z*-**1ra** was consumed much faster than *syn-Z*-**1ra**, directly leading to an increase in R_{sa}. This observation supported the hypothesis that the higher photochemical reactivity of *anti-Z*-**1ra** underlies the light-powered ratcheting behavior of **1ra**, resulting in the enrichment of the *syn-Z* conformer under irradiation.

2.5 | Ultrafast Excited-State Dynamics of 1ra

Time-resolved spectroscopic methods have proven highly effective in elucidating the operating mechanisms of light-driven molecular machines based on photo-isomerizable C═C bonds [42–45]. A representative example was recently reported by Roy and coworkers, who employed ultrafast spectroscopy to investigate the excited-state dynamics of a Feringa-type overcrowded alkene motor possessing push-pull substituents, to elucidate its solvent-dependent photoisomerization behaviors originating from its CT excited-state characters [44].

Here, we investigate the origin of the distinct photochemical reactivities of *anti-* and *syn-Z*-**1ra** using femtosecond transient absorption (fs-TA) spectroscopy to probe the excited-state dynamics of **1ra**. Figure 6a,d shows the fs-TA spectra of *E*- and *Z*-**1ra** in *n*-hexane, following 300 nm excitation. A shorter excitation wavelength was employed in this experiment because both *E*- and *Z*-**1ra** absorb only weakly at wavelengths longer than 300 nm (Figure S9a), thereby limiting the generation of detectable transient signals upon excitation with longer-wavelength pulses. Both isomers exhibit similar spectral shapes and temporal evolution. The spectra display two dominant excited-state absorption (ESA) bands cantered at approximately 425 and 625 nm. The ESA signal at ~625 nm decays substantially within the first picosecond (ps). Beyond 1 ps, no further spectral evolution is observed, and the entire ESA feature decays within the experimental time window (1 ns), indicating depopulation of the excited state.

The early-time ESA band at ~625 nm is attributed to the Franck–Condon (FC) excited state, which undergoes sub-ps relaxation to the S_1-state minimum. This relaxed state is characterized by an ESA peak at ~425 nm together with a broad ESA feature spanning 500–700 nm. The ~425 nm ESA band coincides with the reported absorption of the dimethoxybenzene radical cation [46], while the broad 500–700 nm feature resembles the radical anion signature of the stilbene-like backbone observed in related systems [47]. These spectral signatures indicate pronounced CT character in the S_1-state minimum of both *E*- and *Z*-**1ra**. This assignment is further supported by measurements on the reference compounds *E*- and *Z*-**1Bu**, in which the electron-withdrawing nitro groups are replaced by *tert*-butyl substituents. In *n*-hexane, the fs-TA spectra of *E*- and *Z*-**1Bu** show only the decay of the FC state, without formation of intermediate species exhibiting CT character at ~425 nm (Figure S16). Consistent with the CT nature of the excited state in **1ra**, its excited-state dynamics are also solvent dependent. In acetonitrile, the 425 nm ESA band exhibits enhanced intensity and a shortened lifetime (Figure S17).

15213765, 0, Downloaded from https://chemistry-europe.onlinelibrary.wiley.com/doi/10.1002/chem.71388 by National Yang Ming Chiao Tung, Wiley Online Library on [30/07/2026]. See the Terms and Conditions (https://onlinelibrary.wiley.com/terms-and-conditions) on Wiley Online Library for rules of use; OA articles are governed by the applicable Creative Commons License

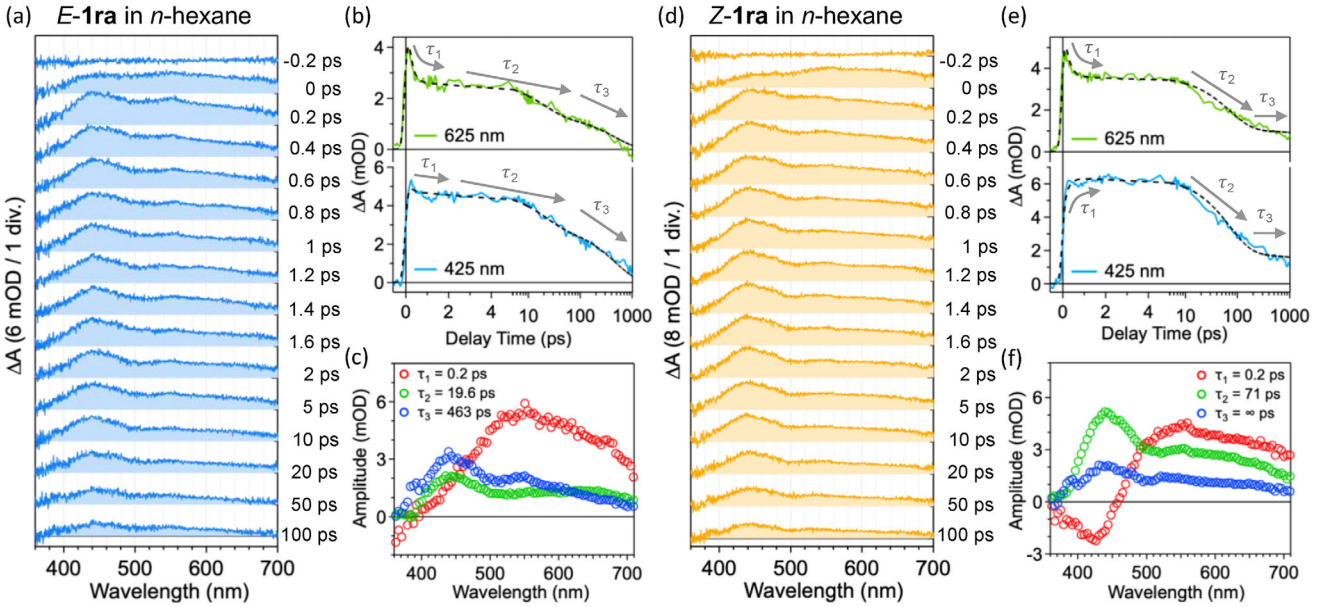

FIGURE 6 | Femtosecond transient absorption spectra of (a) *E*-**1ra** and (d) *Z*-**1ra**. Temporal profiles of the ESA signals at 625 and 425 nm for (b) *E*-**1ra** and (e) *Z*-**1ra**. Black dashed lines indicate the best fits obtained from global fitting. The delay-time region beyond 5 ps is plotted on a logarithmic scale. Corresponding decay-associated spectra (DAS) for (c) *E*-**1ra** and (f) *Z*-**1ra** derived from the global fitting analysis.

To quantitatively analyze the excited-state dynamics of **1ra**, we performed global fitting of the temporal profiles of the transient signals using a sum of three exponential decay functions convoluted with the Gaussian instrumental response function (IRF). The global fitting yields three characteristic time constants: τ_1 = 0.2 ps, τ_2 = 19.6 ps, and τ_3 = 463 ps for *E*-**1ra**; and τ_1 = 0.2 ps, τ_2 = 71 ps, and $\tau_3 = \infty$ ps for *Z*-**1ra**, respectively. Representative fits to the ESA signals at 625 and 425 nm are shown in Figure 6b,e.

The decay-associated spectra (DAS) obtained from the global fitting (Figure 6c,f) provide further insight into the excited-state dynamics. In the τ_1 component, both *E*- and *Z*-**1ra** show a decay of the ESA signal above 500 nm accompanied by a rise below 450 nm. This spectral evolution is characteristic of relaxation from the FC excited state of the stilbene-like backbone to the S_1-state minimum [48]. Such a characteristic feature suggests that the use of a short excitation wavelength does not significantly distort the excited-state dynamics of **1ra**. The τ_2 and τ_3 components reflect the spectral signature of the relaxed S_1 state and correspond to its subsequent depopulation.

The time constants associated with S_1-state decay can be correlated with the photoisomerization dynamics of *E*- and *Z*-**1ra**. For *E*-**1ra**, the two S_1 decay components (τ_2 and τ_3 components in Figure 6c) have comparable amplitudes (approximately 3:2, estimated from the relative intensities at ~425 nm), which can be attributed to two competing $E \rightarrow Z$ isomerization pathways leading to the *syn* and *anti* atropisomers of *Z*-**1ra**. On the other hand, because *Z*-**1ra** exists as a mixture of *syn* and *anti* atropisomers, the observed spectral dynamics may reflect contributions from both species, potentially giving rise to two distinct decay components. Indeed, two S_1 decay components were observed for *Z*-**1ra** (τ_2 and τ_3 components in Figure 6f), although with a more uneven amplitude ratio (~5:2), which can be assigned to contributions from the two atropisomers.

Notably, both decay components are significantly slower than the isomerization of typical *cis*-stilbenes, which occurs on sub-ps timescales [49, 50], indicating the presence of a substantial barrier for S_1-state isomerization in *Z*-**1ra**. Moreover, one of the two S_1 decay components of *Z*-**1ra** occurs on the nanosecond timescale, implying an isomerization pathway that is markedly slower than the other. Comparison with the NMR studies on $Z \rightarrow E$ photoisomerization kinetics of **1ra**, which indicate that photoisomerization of *syn*-*Z*-**1ra** is much slower than that of its *anti*-counterpart, suggests that the slow decay component can be assigned to the isomerization of *syn*-*Z*-**1ra**, whereas the ~72 ps component originates from *anti*-*Z*-**1ra**. The relatively small amplitude of the nanosecond component deviates from the atropisomeric equilibrium ratio at 298 K (K_{sa} = 1.12 in toluene-d_8), implying a reduced branching ratio from the FC excited state to the CT-character S_1 state for *syn*-*Z*-**1ra**.

2.6 | Theoretical Studies

The fs-TA results indicate that the photoisomerization pathways of **1ra** are kinetically biased, which likely governs the stereoselectivity of photoisomerization and underpins the light-powered ratcheting function of **1ra**. To gain further insight into this behavior, we computed the S_1 PES of **1ra** along the C=C torsion coordinate (θ) using TDDFT at the TD-ωB97XD/6-31G*//TD-BHHLYP/6-31G* level [51] to elucidate the energetics associated with C=C isomerization in the excited state. Calculation of this PES was performed on the Gaussian 16 [52] and Q-Chem softwares [53], and the details are described in the Supporting Information (Figures S18–S21). As shown in Figure 7a, both $E \rightarrow Z$ and $Z \rightarrow E$ isomerization pathways encounter a transition state (TS) on the S_1 PES, labeled, respectively, as TS_{in} and TS_{out}. The "in" and "out" subscripts denote the dinitrostyryl unit being inside and outside of the U-shaped cavity of the pentiptycene

15213765, 0, Downloaded from https://chemistry-europe.onlinelibrary.wiley.com/doi/10.1002/chem.71388 by National Yang Ming Chiao Tung, Wiley Online Library on [30/07/2026]. See the Terms and Conditions (https://onlinelibrary.wiley.com/terms-and-conditions) on Wiley Online Library for rules of use; OA articles are governed by the applicable Creative Commons License

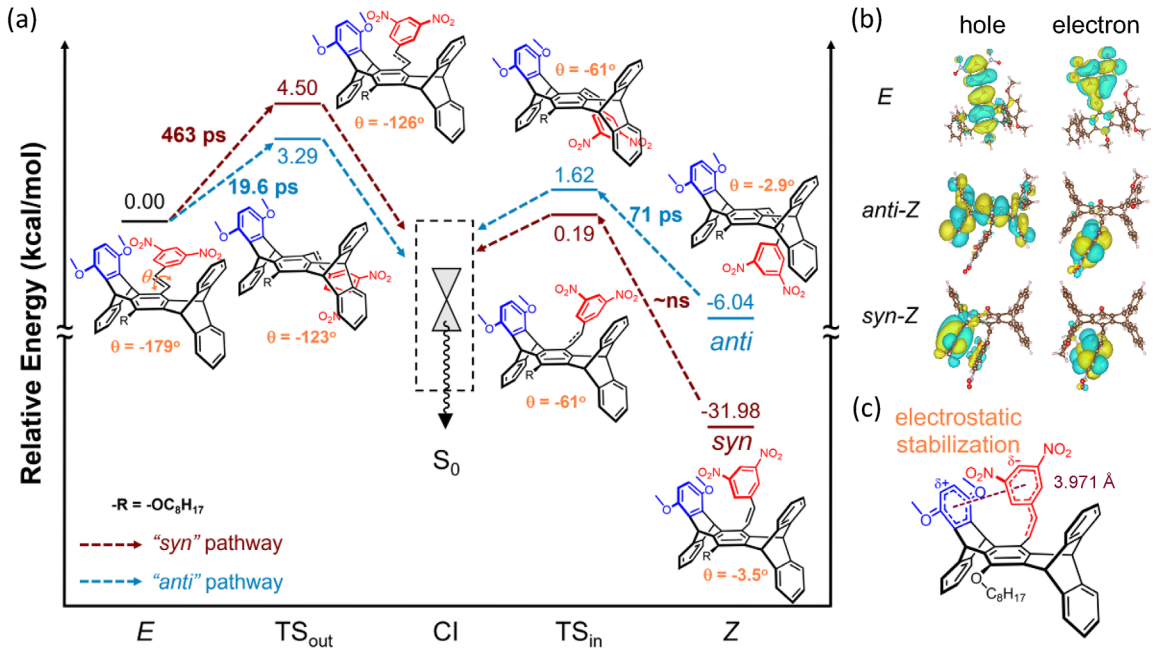

FIGURE 7 | (a) Calculated S_1 PES of **1ra** along the C=C torsion (θ) coordinate. The θ torsion angle for each structure is labeled for reference. For simplicity, the octyloxy groups were replaced with methoxy groups in the calculations. The time signatures associated with each process extrapolated from fs-TA measurements are also provided. (b) Natural transition orbitals (NTOs) of the S_1 states of *E*-, *anti-Z*-, and *syn-Z*-**1ra**. Visualization of orbitals was done with the VESTA software [55]. (c) Schematic illustration of the electrostatic stabilization in the S_1 state of *syn-Z*-**1ra**.

scaffold, respectively [34]. After crossing the TS, the molecule reaches a conical intersection (CI) at approximately $\theta \sim 90°$, where it relaxes back to the S_0 state to form either the *E*- or the *Z*-isomer. For the $E \rightarrow Z$ isomerization, the "*syn* pathway", in which the D–A pair maintains a *syn* orientation, has a predicted barrier of 4.50 kcal/mol, larger than that of the "*anti* pathway" (3.29 kcal/mol). This result could be attributed to the steric hindrance provided by the methoxy substituents. Accordingly, the 19.6 and 463 ps time signatures observed for the S_1-state decay of *E*-**1ra** in fs-TA measurements can be assigned respectively to the *anti* and *syn* pathways. In contrast, the calculated energy barrier of $Z \rightarrow E$ isomerization was substantially larger for the *syn* pathway than for the *anti*-counterpart (32.17 vs. 7.66 kcal/mol). This result aligns with the experimentally observed trend in photochemical reactivity for *syn* versus *anti-Z*-**1ra**, as well as the fs-TA results where the *syn* component follows the slow ns-scale decay. These conclusions support that the light-powered ratcheting behavior of **1ra** originates from the reduced reactivity in *Z*,*E*-photoisomerization for *syn-Z*-**1ra**. Notably, calculations of the corresponding T_1-state PES indicated that the T_1-state minima generally locate near the θ-perpendicular geometries, and that both $E \rightarrow Z$ and $Z \rightarrow E$ isomerization pathways on this surface are essentially barrierless. This result is consistent with the well-established photochemistry of stilbenoids [54], and further suggests that the photoisomerization of **1ra** is unlikely to exhibit stereoselectivity when proceeding through the triplet pathway, as there is effectively no energy barrier to provide kinetic differentiation between the *syn* and *anti* isomerization pathways.

We further performed natural transition orbitals (NTO) analysis on the S_1-state structures of **1ra** described above to investigate their electronic characters. As depicted in Figure 7b, *E*-, *anti-Z*-, and *syn-Z*-**1ra** all exhibit considerable CT character in the S_1 states. Notably, the S_1 state of *syn-Z*-**1ra** is dominated by CT across the D–A pairs, which are in close proximity (inter-centroid distance = 3.971 Å, Figure 7c). Such a spatial arrangement in the *syn-Z* form also leads to pairing of opposite charges, as described in Figure 7c. This provides electrostatic stabilization for *syn-Z*-**1ra** in the excited state, which accounts for its exceptionally high energy barrier for photoisomerization. In other words, the light-powered ratcheting behavior of **1ra** is governed by electrostatic interactions between D–A pairs in the excited state. Remarkably, although such an interaction is absent in the ground state, its influence on the atropisomeric equilibrium of *Z*-**1ra** persists after relaxation back to the ground state.

2.7 | Ratcheting Mechanism and Efficiency

The results above establish **1ra** as an atroposelective light-powered (light-driven) molecular ratchet, where the system absorbs photons and dissipates energy to directionally bias molecular actions [56, 57]. From a mechanistic standpoint, light irradiation not only supplies the energy required to drive the system away from equilibrium but also transfers the stereochemical information of the atropisomers to the photochromic stilbene backbone. From a thermodynamic standpoint, the free energy stored in the 365-nm PSS of **1ra** is estimated to be 19.1 cal/mol of *Z*-**1ra** at 200 K (see Supporting Information for details) [58]). This value is approximately 40% of that reported for the rotaxane-based light-powered information ratchet developed by Leigh and coworkers (49.2 cal/mol at 298 K), which nevertheless exhibited a comparable ratcheting efficiency [59]. This reduction in stored energy arises primarily because the free-energy difference between *syn*- and *anti-Z*-**1ra** (0.13 kcal/mol at 200 K) is only about 40% of that reported for Leigh's system (0.37 kcal/mol at 298 K).

15213765, 0, Downloaded from https://chemistry-europe.onlinelibrary.wiley.com/doi/10.1002/chem.71388 by National Yang Ming Chiao Tung, Wiley Online Library on [30/07/2026]. See the Terms and Conditions (https://onlinelibrary.wiley.com/terms-and-conditions) on Wiley Online Library for rules of use; OA articles are governed by the applicable Creative Commons License

Meanwhile, the excess energy supplied by light is dissipated as heat, generating entropy and ensuring that the overall process obeys the second law of thermodynamics. In this context, the light-induced enrichment of *syn-Z*-**1ra** is consistent with the principle of maximum entropy production (MEP), which predicts that a nonequilibrium steady state sustained by continuous energy input evolves toward the composition that maximizes the rate of entropy production through energy dissipation [60] For **1ra**, this is achieved by increasing the population of *syn-Z*-**1ra**, because this atropisomer predominantly relaxes in the excited state through heat dissipation rather than productive C═C bond twisting. However, heat dissipation may also lead to local photothermal effects [61], which could facilitate C—C bond rotation and thereby reduce the overall ratcheting efficiency. Such an effect likely contributes to the modest experimental ratcheting efficiency, despite the large *syn*/*anti* reactivity difference predicted by theory. In addition, involvement of a triplet-state photoisomerization pathway, which lacks stereoselectivity, may further diminish the ratcheting performance. This effect is particularly relevant for **1ra**, as intersystem crossing is typically efficient in nitro-substituted systems [54, 62]. Finally, limited light penetration in bulk samples may further constrain the ratcheting performance. This limitation could potentially be alleviated by NMR-coupled in situ illumination methods, which provide higher irradiation efficiencies and allow real-time spectroscopic monitoring under continuous light exposure [63–65].

2.8 | Directionality of Light-Driven Rotation

The light-powered atroposelective ratcheting behavior of **1ra** may have implications for the design of autonomous LRMMs. For **1ra**, a photoinduced rotation of the styryl group relative to the pentiptycene scaffold, analogous to that proposed for Curcio's LRMM system [32], can be envisioned (Figure 8). Compared with Curcio's system, **1ra** exhibits a substantially higher atroposelective ratcheting efficiency (±15% vs. ±2% deviation from equilibrium) [32], which we attribute to templated excited-state D–A interactions that enhance photochemical selectivity. Furthermore, steric hindrance within the desymmetrized pentiptycene scaffold imparts inherent structural chirality to **1ra**, introducing a directional bias to the styryl-group rotation associated with atropisomeric interconversion. As illustrated in Figure 8a, when *Z*-**1ra** adopts the 5*R* configuration (atomic numbering as in Figure 2c), the *anti* and *syn* atropisomers preferentially undergo clockwise (CW) and counter-clockwise (CCW) rotations, respectively. Consequently, the net rotational preference is determined jointly by the molecular chirality of the pentiptycene scaffold and the atroposelectivity of the photochemical ratchet. Because **1ra** is *syn*-selective, the preferred overall rotational direction is CCW (Figure 8b). The rotational directionality (D_{rot}) can be estimated as the product of the photochemical ratcheting constant K_r and the directional bias of ground-state rotation (see Supporting Information for details). DFT calculations indicate that approximately 98.8% of the ground-state styryl-group rotation events occur in the preferred direction (Table S2), while K_r = 1.85 at 200 K under 365 nm irradiation. These values yield D_{rot} = 1.83, corresponding to one net directional rotation every 3.4 photochemical cycles. This estimated directionality is substantially greater than that predicted for Curcio's system (D_{rot} = 1.08) [32], highlighting the importance of efficient atroposelective ratcheting in the development of high-performance autonomous LRMMs.

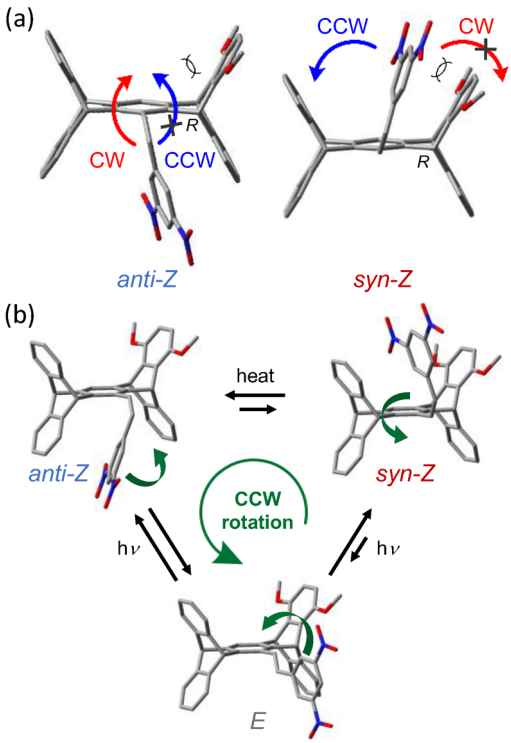

FIGURE 8 | (a) Opposite directional preferences for the ground-state rotation of the styryl group in *anti*- and *syn-Z*-**1ra**, illustrated for the 5*R* configuration of **1ra**. (b) Proposed directional rotation of the styryl group in **1ra** driven by atroposelective photochemical ratcheting. Octyloxy groups are omitted from all structures for clarity.

Although the chirality of the pentiptycene scaffold is fixed, the photochemically induced atroposelectivity in **1ra** may provide a useful handle for directional switching. By incorporating D–A motifs that respond to orthogonal stimuli, such as acid/base inputs, electric fields, or metal coordination, it may be possible to switch the atroposelective ratchet between *syn*- and *anti*-selective modes, thereby reversing the preferred rotational direction. Such stimulus-responsive behavior could broaden the structural and functional scope of light-driven molecular machines [66]. Nevertheless, it should be emphasized that the directional rotation proposed here has not yet been experimentally demonstrated with the same level of rigor as that established for overcrowded-alkene-based LRMMs reported in the literature [22–24]. The present analysis therefore serves primarily to illustrate the potential implications of efficient atroposelective ratcheting, and further experimental studies will be required to substantiate motor-like behavior in this system.

3 | Conclusion

We have demonstrated light-powered atroposelective ratcheting through a stereoselective, reversible photochromic reaction network, with a photochemical ratcheting constant of 1.85. Our results suggest that the ratcheting effect originates from templated excited-state D–A interactions that provide

15213765, 0, Downloaded from https://chemistry-europe.onlinelibrary.wiley.com/doi/10.1002/chem.71388 by National Yang Ming Chiao Tung, Wiley Online Library on [30/07/2026]. See the Terms and Conditions (https://onlinelibrary.wiley.com/terms-and-conditions) on Wiley Online Library for rules of use; OA articles are governed by the applicable Creative Commons License

photochemical differentiation between atropisomeric states. Moreover, we propose that this system holds potential for the design of light-driven autonomous LRMMs. These findings highlight the ability of photochemical processes to differentiate between rapid equilibrating conformers and demonstrate how transient excited-state interactions can be harnessed to influence ground-state behaviors. As the scope of nonequilibrium chemistry continues to grow [67–70], we anticipate that this work will inspire new light-powered ratcheting systems with high levels of complexity and functionality.

Acknowledgments

Financial support for this research was provided by the National Science and Technology Council of Taiwan (NSTC 113-2123-M-002-013; 114-2123-M-002-007; 114-2113-M-007; 114-2811-M-001-015; 114-2113-M-001-022), National Taiwan University (NTU-CC-115L895401). C.-P.H. acknowledges support from Academia Sinica (Grant number AS-IV-114-M01), the Academia Sinica Grid Computing Center (Grant no. AS-CFII-114-A11). We thank Dr. Hsi-Ching Tseng at the NTU Instrumentation Center for the assistance in NMR experiments, and NTU Consortia of Key Technologies for the mass spectrometry technical research services. We thank Mr. Ting-Shen Kuo at the NTNU Instrumentation Center for the assistance in x-ray crystallography. C.-W.C. acknowledges Ms. H.-C. Chang for assistance in graphic design.

Conflicts of Interest

The authors declare no conflicts of interest.

Data Availability Statement

The data that support the findings of this study are available in the Supporting Information of this article.

References

1. M. Kathan and S. Hecht, "Photoswitchable Molecules as Key Ingredients to Drive Systems Away From the Global Thermodynamic Minimum," *Chemical Society Reviews* 46 (2017): 5536–5550, https://doi.org/10.1039/C7CS00112F.

2. B. Sachini, S. Corra, M. Curcio, J. Groppi, and A. Credi, "Defying Chemical Equilibrium With Light," *Trends in Chemistry* 7 (2025): 372–383, https://doi.org/10.1016/j.trechm.2025.04.009.

3. M. Herder and J.-M. Lehn, "The Photodynamic Covalent Bond: Sensitized Alkoxyamines as a Tool To Shift Reaction Networks Out-of-Equilibrium Using Light Energy," *Journal of the American Chemical Society* 140 (2018): 7647–7657, https://doi.org/10.1021/jacs.8b03633.

4. M. Kathan, F. Eisenreich, C. Jurissek, A. Dallmann, J. Gurke, and S. Hecht, "Light-Driven Molecular Trap Enables Bidirectional Manipulation of Dynamic Covalent Systems," *Nature Chemistry* 10 (2018): 1031–1036, https://doi.org/10.1038/s41557-018-0106-8.

5. D. Larsen, P. M. Bjerre, and S. R. Beeren, "Light-controlled Out-of-equilibrium Assembly of Cyclodextrins in an Enzyme-Mediated Dynamic System," *Chemical Communications* 55 (2019): 15037–15040, https://doi.org/10.1039/C9CC08452E.

6. M. Kathan, S. Crespi, N. O. Thiel, et al., "A Light-Fuelled Nanoratchet Shifts a Coupled Chemical Equilibrium," *Nature Nanotechnology* 17 (2022): 159–165, https://doi.org/10.1038/s41565-021-01021-z.

7. J. Wu and J. L. Greenfield, "Photoswitchable Imines Drive Dynamic Covalent Systems to Nonequilibrium Steady States," *Journal of the American Chemical Society* 146 (2024): 20720–20727, https://doi.org/10.1021/jacs.4c03817.

8. J. Wu and J. L. Greenfield, "Harnessing Light to Drive a Non-Photoresponsive Reaction out of Equilibrium," *Chem* (2025): 102579, https://doi.org/10.1016/j.chempr.2025.102579.

9. H. Robson and P. Kovaříček, "Direct Photochemical Control of Imine Exchange Reactions," *Journal of Photochemistry and Photobiology A: Chemistry* 468 (2025): 116490, https://doi.org/10.1016/j.jphotochem.2025.116490.

10. A. Drichel and S. Hecht, "Shifting Merocyanine-Imine Exchange With Visible Light," *Journal of the American Chemical Society* 148 (2026): 6188–6192, https://doi.org/10.1021/jacs.5c17606.

11. J. Vialetto, M. Anyfantakis, S. Rudiuk, M. Morel, and D. Baigl, "Photoswitchable Dissipative Two-Dimensional Colloidal Crystals," *Angewandte Chemie International Edition* 58 (2019): 9145–9149, https://doi.org/10.1002/anie.201904093.

12. X. Jia, C. Shao, X. Bai, et al., "Photoexcitation-Controlled Self-Recoverable Molecular Aggregation for Flicker Phosphorescence," *Proceedings of the National Academy of Sciences* 116 (2019): 4816–4821, https://doi.org/10.1073/pnas.1821991116.

13. T. Bian, Z. Chu, and R. Klajn, "The Many Ways to Assemble Nanoparticles Using Light," *Advanced Materials* 32 (2020): 1905866, https://doi.org/10.1002/adma.201905866.

14. X. Xie, L. Wang, X. Liu, et al., "Light-Powered and Transient Peptide Two-Dimensional Assembly Driven by Trans-to-Cis Isomerization of Azobenzene Side Chains," *Chemical Communications* 56 (2020): 1867–1870, https://doi.org/10.1039/C9CC09448B.

15. M. Weißenfels, J. Gemen, and R. Klajn, "Dissipative Self-Assembly: Fueling With Chemicals Versus Light," *Chem* 7 (2021): 23–37, https://doi.org/10.1016/j.chempr.2020.11.025.

16. H. Lee, J. Tessarolo, D. Langbehn, A. Baksi, R. Herges, and G. H. Clever, "Light-Powered Dissipative Assembly of Diazocine Coordination Cages," *Journal of the American Chemical Society* 144 (2022): 3099–3105, https://doi.org/10.1021/jacs.1c12011.

17. X. Jia and L. Zhu, "Photoexcitation-Induced Assembly: A Bottom-Up Physical Strategy for Driving Molecular Motion and Phase Evolution," *Accounts of Chemical Research* 56 (2023): 655–666, https://doi.org/10.1021/acs.accounts.2c00818.

18. E. Nieland, J. Voss, and B. M. Schmidt, "Shining a Light on Dissipative Supramolecular Assemblies," *Synlett* 34 (2023): 975–982.

19. W. Huang, X. Zhang, H. Su, et al., "Trapping Highly Reactive Photoinduced Charge-Transfer Complex Between Amine and Imide by Light," *Chem* 10 (2024): 2829–2843, https://doi.org/10.1016/j.chempr.2024.05.005.

20. Y. Zhang, X. Liang, C. Yang, Y. Tang, and Q. Yan, "Light-Fueled Non-Photoisomerized Dissipative Self-Assembly System Through Transient Radical-Radical Interactions," *Angewandte Chemie International Edition* 64 (2025): e202512915.

21. I. Neira, C. Taticchi, F. Nicoli, et al., "Light-Driven Ratcheted Formation of Diastereomeric Host-Guest Systems," *Chem* 11 (2025): 102375, https://doi.org/10.1016/j.chempr.2024.11.013.

22. V. García-López, D. Liu, and J. M. Tour, "Light-Activated Organic Molecular Motors and Their Applications," *Chemical Reviews* 120 (2020): 79–124.

23. D. R. S. Pooler, A. S. Lubbe, S. Crespi, and B. L. Feringa, "Designing Light-Driven Rotary Molecular Motors," *Chemical Science* 12 (2021): 14964–14986, https://doi.org/10.1039/D1SC04781G.

24. Z.-J. Chen, H.-F. Lu, C.-W. Chiu, Y.-H. Liu, C.-P. Hsu, and J.-S. Yang, "Extrinsic Gating of the Rotary Direction of a Light-Driven Molecular Motor by Dynamic Boronic Acid–Diol Complexation," *Chemical Science* 16 (2025): 14366–14376, https://doi.org/10.1039/D5SC03240G.

25. S. R. LaPlante, L. D. Fader, K. R. Fandrick, et al., "Assessing Atropisomer Axial Chirality in Drug Discovery and Development," *Journal of Medicinal Chemistry* 54 (2011): 7005–7022, https://doi.org/10.1021/jm200584g.

15213765, 0, Downloaded from https://chemistry-europe.onlinelibrary.wiley.com/doi/10.1002/chem.71388 by National Yang Ming Chiao Tung, Wiley Online Library on [30/07/2026]. See the Terms and Conditions (https://onlinelibrary.wiley.com/terms-and-conditions) on Wiley Online Library for rules of use; OA articles are governed by the applicable Creative Commons License

26. S. Borsley, E. Kreidt, D. A. Leigh, and B. M. W. Roberts, "Autonomous Fuelled Directional Rotation About a Covalent Single Bond," *Nature* 604 (2022): 80–85, https://doi.org/10.1038/s41586-022-04450-5.

27. T.-J. Han, X.-Y. Ke, M.-C. Wang, S.-F. Ni, and G.-J. Mei, "A Chemically Powered Rotary Molecular Motor Based on Reversible Oxazepine Formation," *Angewandte Chemie International Edition* 64 (2025): e202418933, https://doi.org/10.1002/anie.202418933.

28. P.-L. Wang, E. Olivieri, S. Borsley, G. F. S. Whitehead, A. Hasija, and D. A. Leigh, "A Catalysis-Driven Dual Molecular Motor," *Journal of the American Chemical Society* 147 (2025): 10690–10697, https://doi.org/10.1021/jacs.5c01275.

29. J. Berreur, O. F. B. Watts, T. H. N. Bulless, et al., "Redox-Powered Autonomous Directional C–C Bond Rotation Under Enzyme Control," *Nature* 644 (2025): 96–101, https://doi.org/10.1038/s41586-025-09291-6.

30. H.-K. Liu, B. M. W. Roberts, S. Borsley, et al., "Chiral Catalysis-Driven Rotary Molecular Motors," *Nature Chemistry* (2026): 1178–1185.

31. S. Amano, M. Esposito, E. Kreidt, D. A. Leigh, E. Penocchio, and B. M. W. Roberts, "Using Catalysis to Drive Chemistry Away From Equilibrium: Relating Kinetic Asymmetry, Power Strokes, and the Curtin–Hammett Principle in Brownian Ratchets," *Journal of the American Chemical Society* 144 (2022): 20153–20164, https://doi.org/10.1021/jacs.2c08723.

32. F. Nicoli, C. Taticchi, E. Lorini, et al., "Wavelength-Steered Directional Rotation in an Autonomous Light-Driven Molecular Motor," *Nature Chemistry* (2026): 1171–1177, https://doi.org/10.1038/s41557-025-02045-x.

33. J.-S. Yang, Y.-T. Huang, J.-H. Ho, et al., "A Pentiptycene-Derived Light-Driven Molecular Brake," *Organic Letters* 10 (2008): 2279–2282, https://doi.org/10.1021/ol800689a.

34. C.-W. Chiu and J.-S. Yang, "Photoluminescent and Photoresponsive Iptycene-Incorporated π-Conjugated Systems: Fundamentals and Applications," *ChemPhotoChem* 4 (2020): 538–563, https://doi.org/10.1002/cptc.201900300.

35. Y. Li, T. Liu, H. Liu, M.-Z. Tian, and Y. Li, "Self-Assembly of Intramolecular Charge-Transfer Compounds Into Functional Molecular Systems," *Accounts of Chemical Research* 47 (2014): 1186–1198, https://doi.org/10.1021/ar400264e.

36. M. Kumar, K. Venkata Rao, and S. J. George, "Supramolecular Charge Transfer Nanostructures," *Physical Chemistry Chemical Physics* 16 (2014): 1300–1313, https://doi.org/10.1039/C3CP54190H.

37. A. Das and S. Ghosh, "Supramolecular Assemblies by Charge-Transfer Interactions Between Donor and Acceptor Chromophores," *Angewandte Chemie International Edition* 53 (2014): 2038–2054, https://doi.org/10.1002/anie.201307756.

38. B. A. Ikkanda and B. L. Iverson, "Exploiting the Interactions of Aromatic Units for Folding and Assembly in Aqueous Environments," *Chemical Communications* 52 (2016): 7752–7759, https://doi.org/10.1039/C6CC01861K.

39. T. Neveselý, M. Wienhold, J. J. Molloy, and R. Gilmour, "Advances in the E → Z Isomerization of Alkenes Using Small Molecule Photocatalysts," *Chemical Reviews* 122 (2022): 2650–2694, https://doi.org/10.1021/acs.chemrev.1c00324.

40. L. Yu, S. M. Reutzel-Edens, and C. A. Mitchell, "Crystallization and Polymorphism of Conformationally Flexible Molecules: Problems, Patterns, and Strategies," *Organic Process Research & Development* 4 (2000): 396–402, https://doi.org/10.1021/op000028v.

41. L. T. Kuhn and M. Pérez-Trujillo, "Continuous-Wave (CW) Photo-CIDNP NMR Spectroscopy: A Tutorial," *Magnetic Resonance in Chemistry* 63 (2025): 1020–1034, https://doi.org/10.1002/mrc.70031.

42. R. Wilcken, M. Schildhauer, F. Rott, et al., "Complete Mechanism of Hemithioindigo Motor Rotation," *Journal of the American Chemical Society* 140 (2018): 5311–5318, https://doi.org/10.1021/jacs.8b02349.

43. P. Roy, A. S. Sardjan, W. Danowski, W. R. Browne, B. L. Feringa, and S. R. Meech, "Photophysics of First-Generation Photomolecular Motors: Resolving Roles of Temperature, Friction, and Medium Polarity," *Journal of Physical Chemistry A* 125 (2021): 1711–1719, https://doi.org/10.1021/acs.jpca.0c11050.

44. P. Roy, A. S. Sardjan, W. Danowski, W. R. Browne, B. L. Feringa, and S. R. Meech, "Control of Photoconversion Yield in Unidirectional Photomolecular Motors by Push–Pull Substituents," *Journal of the American Chemical Society* 145 (2023): 19849–19855, https://doi.org/10.1021/jacs.3c06070.

45. M. Hartinger, M. Herm, C. Schüßlbauer, et al., "From Triplet to Twist: The Photochemical E/Z-Isomerization Pathway of the Near-Infrared Photoswitch Peri -Anthracenethioindigo," *Angewandte Chemie International Edition* 64 (2025): e202510626, https://doi.org/10.1002/anie.202510626.

46. S. M. Hubig, W. Jung, and J. K. Kochi, "Cation Radicals as Intermediates in Aromatic Halogenation With Iodine Monochloride: Solvent and Salt Effects on the Competition Between Chlorination and Iodination," *Journal of Organic Chemistry* 59 (1994): 6233–6244, https://doi.org/10.1021/jo00100a025.

47. W.-T. Sun, S.-L. Huang, H.-H. Yao, I. C. Chen, Y.-C. Lin, and J.-S. Yang, "An Antilock Molecular Braking System," *Organic Letters* 14 (2012): 4154–4157, https://doi.org/10.1021/ol3018193.

48. H. Kuramochi, T. Tsutsumi, K. Saita, et al., "Ultrafast Raman Observation of the Perpendicular Intermediate Phantom State of Stilbene Photoisomerization," *Nature Chemistry* 16 (2024): 22–27, https://doi.org/10.1038/s41557-023-01397-6.

49. S. Takeuchi, S. Ruhman, T. Tsuneda, M. Chiba, T. Taketsugu, and T. Tahara, "Spectroscopic Tracking of Structural Evolution in Ultrafast Stilbene Photoisomerization," *Science* 322 (2008): 1073–1077, https://doi.org/10.1126/science.1160902.

50. C. Wang, M. D. J. Waters, P. Zhang, et al., "Different Timescales During Ultrafast Stilbene Isomerization in the Gas and Liquid Phases Revealed Using Time-Resolved Photoelectron Spectroscopy," *Nature Chemistry* 14 (2022): 1126–1132, https://doi.org/10.1038/s41557-022-01012-0.

51. A. D. Becke, "A New Mixing of Hartree–Fock and Local Density-Functional Theories," *Journal of Chemical Physics* 98 (1993): 1372–1377.

52. M. J. Frisch, G. W. Trucks, H. B. Schlegel, et al., (2016), *Gaussian 16 Rev. C.01*.

53. Y. Shao, Z. Gan, E. Epifanovsky, et al., "Advances in Molecular Quantum Chemistry Contained in the Q-Chem 4 Program Package," *Molecular Physics* 113 (2015): 184–215, https://doi.org/10.1080/00268976.2014.952696.

54. D. H. Waldeck, "Photoisomerization Dynamics of Stilbenes," *Chemical Reviews* 91 (1991): 415–436, https://doi.org/10.1021/cr00003a007.

55. K. Momma and F. Izumi, "VESTA: A Three-Dimensional Visualization System for Electronic and Structural Analysis," *Journal of Applied Crystallography* 41 (2008): 653–658, https://doi.org/10.1107/S0021889808012016.

56. T. Sangchai, S. Al Shehimy, E. Penocchio, and G. Ragazzon, "Artificial Molecular Ratchets: Tools Enabling Endergonic Processes," *Angewandte Chemie International Edition* 62 (2023): e202309501.

57. S. Borsley, D. A. Leigh, and B. M. W. Roberts, "Molecular Ratchets and Kinetic Asymmetry: Giving Chemistry Direction," *Angewandte Chemie International Edition* 63 (2024): e202400495, https://doi.org/10.1002/anie.202400495.

58. L. Binks, S. Borsley, T. R. Gingrich, D. A. Leigh, E. Penocchio, and B. M. W. Roberts, "The Role of Kinetic Asymmetry and Power Strokes in an Information Ratchet," *Chem* 9 (2023): 2902–2917, https://doi.org/10.1016/j.chempr.2023.05.035.

59. V. Serreli, C.-F. Lee, E. R. Kay, and D. A. Leigh, "A Molecular Information Ratchet," *Nature* 445 (2007): 523–527, https://doi.org/10.1038/nature05452.

60. R. G. Endres, "Entropy Production Selects Nonequilibrium States in Multistable Systems," *Scientific Reports* 7 (2017): 14437.

15213765, 0, Downloaded from https://chemistry-europe.onlinelibrary.wiley.com/doi/10.1002/chem.71388 by National Yang Ming Chiao Tung, Wiley Online Library on [30/07/2026]. See the Terms and Conditions (https://onlinelibrary.wiley.com/terms-and-conditions) on Wiley Online Library for rules of use; OA articles are governed by the applicable Creative Commons License

61. L. Zhao, Y. Liu, R. Xing, and X. Yan, "Supramolecular Photothermal Effects: A Promising Mechanism for Efficient Thermal Conversion," *Angewandte Chemie International Edition* 59 (2020): 3793–3801, https://doi.org/10.1002/anie.201909825.

62. W. Rodríguez-Córdoba, L. Gutiérrez-Arzaluz, F. Cortés-Guzmán, and J. Peon, "Excited State Dynamics and Photochemistry of Nitroaromatic Compounds," *Chemical Communications* 57 (2021): 12218–12235, https://doi.org/10.1039/D1CC04999B.

63. A. Seegerer, P. Nitschke, and R. M. Gschwind, "Combined In Situ Illumination-NMR-UV/Vis Spectroscopy: A New Mechanistic Tool in Photochemistry," *Angewandte Chemie International Edition* 57 (2018): 7493–7497, https://doi.org/10.1002/anie.201801250.

64. Y. Ji, D. A. DiRocco, J. Kind, C. M. Thiele, R. M. Gschwind, and M. Reibarkh, "LED-Illuminated NMR Spectroscopy: A Practical Tool for Mechanistic Studies of Photochemical Reactions," *ChemPhotoChem* 3 (2019): 984–992, https://doi.org/10.1002/cptc.201900109.

65. J. E. Bramham and A. P. Golovanov, "Sample Illumination Device Facilitates In Situ Light-Coupled NMR Spectroscopy Without Fibre Optics," *Communications Chemistry* 5 (2022): 90, https://doi.org/10.1038/s42004-022-00704-5.

66. M. Jeong, J. Park, and S. Kwon, "Molecular Switches and Motors Powered by Orthogonal Stimuli," *European Journal of Organic Chemistry* 2020 (2020): 7254–7283, https://doi.org/10.1002/ejoc.202001179.

67. J. H. van Esch, R. Klajn, and S. Otto, "Chemical Systems out of Equilibrium," *Chemical Society Reviews* 46 (2017): 5474–5475..

68. R. Plasson and L. Jullien, "Steady Out-of-Equilibrium Chemistry: What? Why? How?," *ChemSystemsChem* 7 (2025): e202500011, https://doi.org/10.1002/syst.202500011.

69. C. Cheng, P. R. McGonigal, J. F. Stoddart, and R. D. Astumian, "Design and Synthesis of Nonequilibrium Systems," *ACS Nano* 9 (2015): 8672–8688, https://doi.org/10.1021/acsnano.5b03809.

70. Y. Feng, M. Ovalle, J. S. W. Seale, et al., "Molecular Pumps and Motors," *Journal of the American Chemical Society* 143 (2021): 5569–5591, https://doi.org/10.1021/jacs.0c13388.

71. J.-S. Yang, K.-L. Liau, C.-M. Wang, and C.-Y. Hwang, "Substituent-Dependent Photoinduced Intramolecular Charge Transfer in N-Aryl-Substituted Trans-4-Aminostilbenes," *Journal of the American Chemical Society* 126 (2004): 12325–12335, https://doi.org/10.1021/ja047604d.

72. X.-Z. Zhu and C.-F. Chen, "Iptycene Quinones: Synthesis and Structure," *Journal of Organic Chemistry* 70 (2005): 917–924, https://doi.org/10.1021/jo0483015.

73. H. Jian and J. M. Tour, "Preparative Fluorous Mixture Synthesis of Diazonium-Functionalized Oligo(phenylene vinylene)s," *Journal of Organic Chemistry* 70 (2005): 3396–3424, https://doi.org/10.1021/jo048051s.

74. W.-T. Sun, Y.-T. Huang, G.-J. Huang, et al., "Pentiptycene-Derived Light-Driven Molecular Brakes: Substituent Effects of the Brake Component," *Chemistry—A European Journal* 16 (2010): 11594–11604, https://doi.org/10.1002/chem.201000764.

75. Y. Zhao and D. G. Truhlar, "Density Functionals With Broad Applicability in Chemistry," *Accounts of Chemical Research* 41 (2008): 157–167, https://doi.org/10.1021/ar700111a.

76. Y. Ji, D. A. DiRocco, C. M. Hong, M. K. Wismer, and M. Reibarkh, "Facile Quantum Yield Determination via NMR Actinometry," *Organic Letters* 20 (2018): 2156–2159, https://doi.org/10.1021/acs.orglett.8b00391.

77. H. Lemmetyinen, N. V. Tkachenko, A. Efimov, and M. Niemi, "Photoinduced Intra- and Intermolecular Electron Transfer in Solutions and in Solid Organized Molecular Assemblies," *Physical Chemistry Chemical Physics* 13 (2011): 397–412, https://doi.org/10.1039/C0CP01106A.

78. Y. Shao, M. Head-Gordon, and A. I. Krylov, "The Spin–Flip Approach Within Time-Dependent Density Functional Theory: Theory and Applications to Diradicals," *Journal of Chemical Physics* 118 (2003): 4807–4818, https://doi.org/10.1063/1.1545679.

Supporting Information

Additional supporting information can be found online in the Supporting Information section.

The authors have cited additional references within the Supporting Information [71–78]. Additional supporting information can be found online in the Supporting Information section. CCDC 2523958 contains the supplementary crystallographic data for this paper, which can be obtained free of charge from The Cambridge Crystallographic Data Centre via www.ccdc.cam.ac.uk/structures.

Supporting File 1: chem71388-sup-0001-SuppMat.pdf.

15213765, 0, Downloaded from https://chemistry-europe.onlinelibrary.wiley.com/doi/10.1002/chem.71388 by National Yang Ming Chiao Tung, Wiley Online Library on [30/07/2026]. See the Terms and Conditions (https://onlinelibrary.wiley.com/terms-and-conditions) on Wiley Online Library for rules of use; OA articles are governed by the applicable Creative Commons License